Capture numbers and island size distributions in models of submonolayer surface growth

Martin Körner, Mario Einax,* and Philipp Maass†
Fachbereich Physik, Universität Osnabrück, Barbarastraße 7, 49076 Osnabrück, Germany
(Received 27 May 2012; published 2 August 2012)

The capture numbers entering the rate equations (RE) for submonolayer film growth are determined from extensive kinetic Monte Carlo (KMC) simulations for simple representative growth models yielding point, compact, and fractal island morphologies. The full dependence of the capture numbers $\sigma_s(\Theta,\Gamma)$ on island size s and on both the coverage Θ and the $\Gamma = D/F$ ratio between the adatom diffusion coefficient D and deposition rate F is determined. Based on this information, the RE are solved to give the RE island size distribution (RE-ISD), as quantified by the number $n_s(\Theta,\Gamma)$ of islands of size s per unit area. The RE-ISDs are shown to agree well with the corresponding KMC-ISDs for all island morphologies. For compact morphologies, however, this agreement is only present for coverages smaller than $\Theta \simeq 5\%$ due to a significantly increased coalescence rate compared to fractal morphologies. As found earlier, the scaled KMC-ISDs $n_s\bar{s}^2/\Theta$ as a function of scaled island size $x = s/\bar{s}$ approach, for fixed Θ, a limiting curve $f_\infty(x,\Theta)$ for $\Gamma \to \infty$. Our findings provide evidence that the limiting curve is independent of Θ for point islands, while the results for compact and fractal island morphologies indicate a dependence on Θ.

DOI: 10.1103/PhysRevB.86.085403 PACS number(s): 81.15.Aa, 68.55.A−, 68.55.−a

I. INTRODUCTION

The kinetics of submonolayer nucleation and island growth during the initial stage of epitaxial thin film growth has been studied intensively both experimentally and theoretically for more than three decades (for reviews, see Refs. 1–4, and references therein). Important aspects of the growth kinetics in the submonolayer growth regime can be described by the rate equations (RE) approach.[5] This approach has proven to be very valuable in inorganic thin film growth. Interestingly, many of the theoretical concepts developed for thin film growth kinetics of inorganic materials, have shown recently to be very valuable also for applications in organic thin film growth.[6–10] This is due to the fact that these concepts often are not specifically referring to particular materials. Instead, they take into account the key mechanisms involved in the complex interplay of deposition, evaporation, diffusion, aggregation and dissociation from a general viewpoint.

Parameters entering the RE are the capture numbers $\sigma_s(\Theta,\Gamma)$, which describe the strength of islands of size s to capture adatoms at a coverage Θ and ratio $D/F \equiv \Gamma$ of the adatom diffusion coefficient D and deposition flux F. The dependence of the capture numbers on s has been studied for various Γ but only for one or a few Θ values. In this work, we present a systematic study of the full dependence on both Θ and Γ for different types of island morphologies and the case, where detachments of atoms from islands can be neglected, corresponding to a critical nucleus of size $i = 1$. This is motivated by the following questions, which have not been thoroughly answered yet. (1) If the $\sigma_s(\Theta,\Gamma)$ are known, do the RE then predict correctly the number density $n_s(\Theta,\Gamma)$ of islands of size s, that means the island size distribution (ISD)? This question indeed was earlier posed by Ratsch and Venables[11] as well as Evans *et al.*[3] The answer to this question is not obvious, since the RE with known capture numbers $\sigma_s(\Theta,\Gamma)$ neglect many-particle correlation effects,[12] spatial fluctuations in shapes and capture zones of islands, and coalescence events that, despite rare in the early-stage growth, can have a significant influence.[13] (2) Is there a simple functional form of the $\sigma_s(\Theta,\Gamma)$, in particular, is there a scaling of these capture numbers with respect to an effective capture length as suggested by a self-consistent treatment[14,15] based on the RE? Do the σ_s, when scaled with respect to their mean $\bar{\sigma}$, depend for large Γ on the scaled island size $s/\bar{s}$ only, as suggested by Bartelt and Evans?[16]

In previous studies, it has been found that the scaled ISD $\bar{s}^2 n_s/\Theta$ as a function of scaled island size $x = s/\bar{s}$ approaches, for fixed coverage Θ, a scaling function $f(x)$ for large Γ. Early simulations suggested that $f(x)$ is independent of Θ and moreover not sensitive to the island morphology. However, later results showed[3,16] that the morphology has an influence on the form of $f(x)$. In fact, one would expect the scaling function $f(x)$ to become independent of Θ if the RE with known capture numbers correctly predict the ISD, and if the scaled capture numbers $\sigma/\bar{\sigma}$ as a function of $s/\bar{s}$ become independent of Θ for large Γ. Under these assumptions, an explicit relation was proposed by Bartelt and Evans,[16,17] which connects the scaling function of the capture numbers with the scaling function of the ISD. We hence address the following further questions: (3) is the scaling function $f(x)$ independent of Θ for large Γ? What is the influence of the island morphology? Can the relation between the scaled ISD $f(x)$ and the scaling function for the capture numbers be confirmed?

The RE treatment is based on a coupled set of simple rate equations describing the time evolution of the adatom density n_1 and the number density n_s of islands with size $s \geqslant 2$, if spatial correlations among islands during growth are neglected. Taking into account direct impingement of arriving atoms at the border of islands, the RE for the case $i = 1$ read

$$\frac{1}{F}\frac{\mathrm{d}n_1}{\mathrm{d}t} = (1-\Theta) - 2\Gamma\sigma_1 n_1^2 - \Gamma n_1 \sum_{s>1}\sigma_s n_s - 2\kappa_1 n_1 - \sum_{s>1}\kappa_s n_s, \quad (1)$$

$$\frac{1}{F}\frac{\mathrm{d}n_s}{\mathrm{d}t} = \Gamma n_1(\sigma_{s-1}n_{s-1} - \sigma_s n_s) + \kappa_{s-1}n_{s-1} - \kappa_s n_s, \quad s = 2,3,\ldots. \quad (2)$$

These equations refer to the precoalescence regime where only adatoms are mobile and it is presumed that reevaporation of atoms and atom movements between the first and second layers can be disregarded. Moreover, adatoms arriving on top of an island are not counted, i.e., s in a strict sense refers to the number of substrate sites covered by an island (or the island area). The coverage Θ entering Eq. (1) is given by $\Theta = \sum_{s\geqslant 1} s n_s = 1 - \exp(-Ft)$ and takes into account that adatoms are generated by deposition into the uncovered substrate area (as common in the literature in this field, we set the length unit equal to the the size of the substrate lattice unit). The terms with $\sigma_1(\Theta)$ and $\kappa_1(\Theta)$ describe the nucleation of dimers due to attachment of two adatoms by diffusion and due to direct impingement, respectively. The term $\propto n_1\sigma_s n_s$ describes the attachment of adatoms to islands of size $s > 1$, and the term $\propto \kappa_s n_s$ the direct impingement of deposited atoms to boundaries of islands with size s. For the idealized point island model, s refers to the total number of atoms that arrived at a point, and $(1 - \Theta)$ in Eq. (1) is replaced by one (no covered substrate area). For a unified discussion of capture numbers and the ISD, we formally set $\Theta = Ft$ for the point island model.

Introducing the total number density of stable islands N and the average capture number $\overline{\sigma}$,

$$N = \sum_{s>1} n_s, \quad \overline{\sigma} = \frac{1}{N}\sum_{s>1}\sigma_s n_s, \tag{3}$$

a reduced set of equations for $n_1(\Theta)$ and $N(\Theta)$ can be derived from Eqs. (1) and (2) within the RE treatment. These equations predict the scaling relation $N \propto \Gamma^{-\chi}$ with the scaling exponent $\chi = 1/3$.[18,19] This relation has been successfully validated by several growth experiments in the past and applied to extract adatom diffusion barriers and binding energies in metal epitaxy. A discussion of many of these experiments can be found in Ref. 2. Recently, the relation has also been applied in organic thin film growth.[6,7] An extended RE approach for multicomponent adsorbates[4,20] was recently suggested to determine binding energies between unlike atoms from island density data.[21]

More detailed information on the growth kinetics is contained in the ISD. If the full dependence of the ISD $n_s(\Theta,\Gamma)$ on Θ and Γ is mediated by the mean island size $\bar{s}(\Theta,\Gamma)$, the ISD should obey the following scaling form, as first suggested by Vicsek and Family,[22]

$$\frac{\bar{s}^2(\Theta,\Gamma)}{\Theta} n_s(\Theta,\Gamma) = f\left(\frac{s}{\bar{s}(\Theta,\Gamma)}\right). \tag{4}$$

Here, the scaling function $f(x)$ must fulfill the conditions $\int_0^\infty f(x)dx = \int_0^\infty x f(x)dx = 1$. The scaling behavior was found to give a good effective description for large Γ. More precisely, the curves $\bar{s}^2 n_s/\Theta$ as a function of $x = s/\bar{s}$ approach a limiting curve,[23]

$$\lim_{\Gamma\to\infty} \frac{\bar{s}^2}{\Theta} n_{x\bar{s}}(\Theta,\Gamma) = f_\infty(x,\Theta)\,. \tag{5}$$

Previous studies for a few fixed Θ values suggest that $f_\infty(x,\Theta)$ is independent of Θ.

An explicit expression for the scaling function $f(x)$ with shape independent of Θ was suggested by Amar and Family,[24]

$$f(x) = C_i x^i \exp(-i a_i x^{1/a_i}). \tag{6}$$

The parameters entering this scaling function depend on the size of the critical nucleus i, which allows one to determine i in experiments.[7,9,25,26] Equation (6) was believed to be independent even of the morphology;[24] but this has later been questioned.[3,16]

Based on a continuum limit of the RE (2) and scaling assumptions for the capture numbers and a neglect of the Θ dependence, an expression for the limiting curve $f_\infty(x)$ was derived by Bartelt and Evans,[16,17]

$$f_\infty(x) = f_\infty(0)\exp\left[\int_0^x \mathrm{d}y \frac{(2z_\infty - 1) - C'_{\mathrm{tot}}(y)}{C_{\mathrm{tot}}(y) - zy}\right], \tag{7}$$

where $z_\infty = \partial(\ln\bar{s})/\partial(\ln\Theta)$ and $C_{\mathrm{tot}}(x)$ is a linear combination of the scaled capture numbers $C_\infty(x) = \sigma_s/\bar{\sigma}$ and scaled direct capture areas $K_\infty(x) = \kappa_s/\bar{\kappa}$. The "$\infty$" subscript indicates that the large $\Gamma \to \infty$ limit should be taken. As pointed out by Bartelt and Evans, $C_{\mathrm{tot}}(x)$ should be well approximated by the scaled capture numbers alone, $C_{\mathrm{tot}}(x) \approx (1 - \Theta)C_\infty(x)$. In Appendix A, we show that in fact it holds $C_{\mathrm{tot}}(x) \approx C_\infty(x)$. The two conditions for $f_\infty(x)$ (normalization and first moment equal to one) imply that $C_\infty(0) = (1 - z)/f_\infty(0)$ and $\int_0^\infty dx\, C_\infty(x) f_\infty(x) = 1$.[3,17]

It is interesting to note that a semiempirical form, which has a structure similar to Eq. (6) has been suggested recently by Pimpinelli and Einstein[27] for the distribution of capture zones A as identified by Voronoi tessellation,

$$P_\beta = c_\beta a^\beta \exp(-d_\beta a^2)\,, \tag{8}$$

where $a = A/\bar{A}$ is the rescaled capture zone with respect to the mean $\bar{A}$ and $\beta = i + 1$ (see also Ref. 28). This distribution corresponds to a generalized Wigner surmise from random matrix theory. The parameter $\beta = i + 1$ and the functional form, however, are controversially discussed.[29,30]

Besides this recent progress in predicting functional forms of capture zone distributions, there are only a few studies so far[13,31,32] that address the problem whether an integration of the REs (1) and (2) can yield correctly the ISD for different cluster morphologies in the precoalescence regime. For an integration of the RE, a reliable determination of $\sigma_s(\Theta,\Gamma)$ is needed. Four general approaches have been followed for this purpose: (i) within a self-consistent ansatz one can solve the diffusion field around an island and derive determining equations for the capture numbers by equating the attachment currents of the diffusion field and the RE.[14,15] (ii) By modeling the island growth with the level set method,[33] one can analogously equate attachments currents and determine the capture numbers.[31,32] (iii) Balancing the deposition rate $FA_s n_s$ into the mean capture zone A_s of islands of size s with the RE expression $D\sigma_s n_1 n_s$ for the attachment rate to these islands, yields $\sigma_s \simeq A_s/\Gamma n_1$. This means that the capture numbers can be approximately calculated from a determination of the A_s, e.g., by Voronoi tessellation.[17,34–36] (iv) In simulations, where the individual attachments are followed, the capture numbers can be calculated from the mean number of attachments M_s to island of size s during a time interval Δt [see Eq. (9) and the discussion in Sec. II].[16]

The paper is organized as follows. First, we describe in Sec. II the method used to generate point, compact and fractal island morphologies, and the method for determining the capture numbers as function of island size and coverage. In Sec. III, we discuss the results for the capture numbers and compare these with the prediction of the self-consistent theory. In Sec. IV, we analyze the mean island and adatom densities for the different island morphologies and discuss their prediction by the self-consistent RE and the RE based on the capture numbers determined in the KMC simulations. In Sec. V, we demonstrate that the ISD is successfully predicted by the RE as long as coalescence events can be neglected. These coalescence events are relevant already for small coverages $\Theta \gtrsim 0.05$ for compact morphologies, while they turn out to be much less important for fractal morphologies. The reason for these differences are reduced coalescence rates for fractal island morphologies because of a screening effect.[1,37] Finally, we study in Sec. VI the behavior of the scaled capture numbers and scaled ISDs in the limit $\Gamma \to \infty$.

II. SUBMONOLAYER GROWTH: MODELS, MORPHOLOGIES AND SIMULATIONS

The KMC simulations are performed with a first reaction time Monte Carlo algorithm[38,39] on a square lattice with $L \times L$ sites. In this algorithm, two times τ_F and τ_D are randomly generated from the exponential probability density $\psi(\tau) = \gamma \exp(-\gamma\tau)$, where $\gamma = L^2F$ for τ_F, corresponding to a deposition process, and $\gamma = 4DL^2n_1$ for τ_D, corresponding to one of the possible diffusive jumps of adatoms. If $\tau_D < \tau_F$, the simulation time is incremented by τ_D and one of the L^2n_1 adatoms is selected randomly and moved to a randomly selected vacant nearest neighbor site. If $\tau_F < \tau_D$, the simulation time is incremented by τ_F and one of the L^2 sites is randomly chosen. If this site is vacant, an additional adatom is deposited on this site, while, if the site is occupied, no deposition takes place.

With respect to the formation of islands, we consider three simple growth models that are representative for the different types of island morphologies in the case of $i = 1$. Fractal islands are generated by applying "hit and stick" aggregation, which means an adatom having another atom as the nearest neighbor becomes immobilized. Compact island morphologies are produced by letting islands grow spirally into a quadratic form as in Ref. 40, meaning that each adatom attached to an island is displaced to the corresponding tip of the spiral. Point island morphologies are generated by displacing an adatom attaching to an island to the site representing the island, while bookkeeping the total number of aggregated atoms for the island size.

To calculate the capture numbers σ_s at the coverage Θ, we use the following procedure, which is based on the method outlined in Ref. 16; each simulation run is stopped at coverage Θ and the number densities $n_s = N_s/L^2$, $s = 1,2,\ldots$ are determined, where N_s are the numbers of monomers ($s = 1$) and islands ($s > 1$). Then the simulation is continued for a time interval Δt without deposition and the following additional rules are implemented: (i) if an adatom is attaching to an island of size $s > 1$, a counter M_s is incremented and the adatom thereafter repositioned at a randomly selected site on the free substrate area (i.e., a site which is neither covered nor the nearest neighbor of a covered site), and (ii) if two adatoms form a dimer, a counter M_1 is incremented and the two adatoms thereafter are repositioned randomly as described in (i). In this way, a stationary state is maintained at the coverage Θ. The mean attachment rate per unit area to islands of size s is $M_s/(L^2\Delta t)$, and equating this with the expression $D\sigma_s n_s n_1$ from the RE (1, 2) yields

$$\sigma_s = \frac{M_s}{L^2 \Delta t D n_s n_1}, \quad s = 1,2,\ldots. \tag{9}$$

Averaging over many simulation runs (configurations) gives $\sigma_s(\Theta,\Gamma)$. The κ_s are determined from the lengths of the islands boundaries, which are simultaneously monitored during the simulation and averaged for each size s.

The continuous-time Monte Carlo (KMC) simulations are performed on a square lattice with periodic boundary conditions and $L \times L = 8000 \times 8000$ sites for four different $\Gamma = 10^5$, 10^6, 10^7, and 10^8. For each value of Θ, an average over 10^8 nucleation/attachment events was performed.

III. CAPTURE NUMBERS

The direct capture areas for point islands on a square lattice are given by $\kappa_s = 4$. For compact and fractal islands, the κ_s increase as $\sim\sqrt{s}$ and $\sim s$, respectively, and their dependence on Θ and Γ is very weak. Representative results for the capture numbers σ_s are shown in Fig. 1 as a function of s for fixed

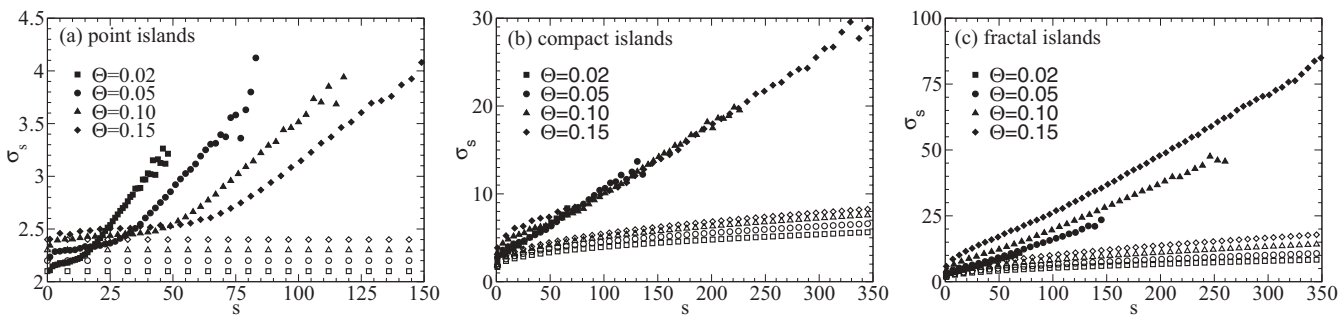

FIG. 1. Capture numbers as a function of s for $\Gamma = 10^7$ and four different fixed coverages for the models representing (a) point, (b) compact, and (c) fractal island morphologies. The filled symbols refer to the σ_s obtained from the KMC simulations and the open symbols to the results of the self-consistent theory according to Eqs. (10) (with the R_s taken from the simulations, see text and Fig. 3).

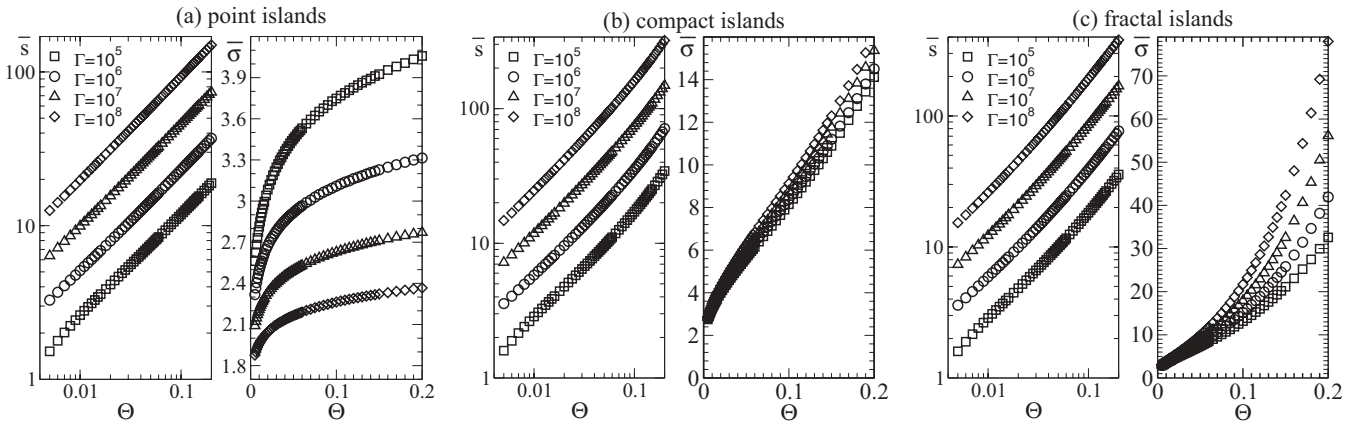

FIG. 2. Mean capture number $\bar{\sigma}$ and mean island size $\bar{s}$ as a function of Θ for the four simulated Γ values and the models representing point, compact, and fractal island morphologies.

$\Gamma = 10^7$ and four different coverages for the (a) point, (b) compact, and (c) fractal island morphologies. For the other simulated Γ values, a similar behavior was obtained. The mean $\bar{\sigma}(\Theta,\Gamma)$ [see Eq. (3)] as a function of Θ for all simulated Γ values is displayed in Fig. 2, together with the mean island size $\bar{s}(\Theta,\Gamma)$. These functions are later used in Sec. VI when investigating the scaled capture numbers σ_s in connection with the scaled island densities in the limit $\Gamma \to \infty$.

A common feature for all morphologies in Fig. 1 is a linear increase of σ_s with s for large $s > \bar{s}$. It can be understood[3] from the proportionality of the σ_s to the mean capture zone areas A_s, and the fact that large islands typically exhibit large A_s, which led to the stronger growth of these islands. Since a twice as large capture zone gives on average rise to a twice as large island, it holds $A_s \sim s$ and hence $\sigma_s \propto A_s \sim s$.[3,16]

With respect to the dependence on the coverage Θ, the σ_s in Fig. 1 have a quite different behavior for the three morphologies in the regime $s > \bar{s}$. While for the point islands the σ_s decrease with Θ, they are almost independent of Θ for the compact islands, and they increase with Θ for the fractal islands. Main reason for these differences is that for point islands the number density N continues to increase with Θ (that means time $t = \Theta/F$) due to ongoing nucleation of new islands, while for compact and fractal morphologies, N tends to saturate for larger Θ, with less pronounced saturation in the compact case (see Sec. IV below). During the growth in the point island model, a large capture zone surrounding a large island is, compared to the other two morphologies, more frequently destroyed by a nucleation event in this zone, and the $A_s \propto \sigma_s$ thus decrease with Θ for fixed $s > \bar{s}$. Due to the higher nucleation rate and the missing spatial extension of islands in the point island model, the corresponding σ_s are much smaller than for the compact and fractal morphologies. The larger island extension and the strong capture of adatoms by finger tips in the case of fractal islands lead to about five times larger σ_s in comparison to the compact islands.

The differences with respect to the Θ dependence are also reflected in the behavior of $\bar{\sigma}(\Theta,\Gamma)$ in Fig. 2. In fact, when considering the scaled capture numbers $\sigma_s/\bar{\sigma}$, the Θ dependence for $s > \bar{s}$ becomes qualitatively the same for all morphologies (increase of $\sigma_s/\bar{\sigma}$ with Θ, see Sec. VI below). For small $s < \bar{s}$, the curves in Fig. 1 show a nonlinear dependence of σ_s on s for all morphologies.[35,41,42] By combining the linear function for large s with a polynomial at small s, we fitted the results for σ_s for all simulated Θ and Γ values. These fits, together with corresponding fits for the κ_s, were used to integrate the REs (1) and (2).

The mean island size $\bar{s}$ in Fig. 2 reproduces the behavior seen in many earlier studies.[3] In the point island model the straight lines in the double logarithmic representation are in agreement with $\bar{s} \sim \Theta^z$ with $z = 2/3$ as predicted by a scaling analysis of the reduced RE.[3,43,44] In the case of the compact and fractal island morphologies, the slope $z(\Theta) = \partial \ln \bar{s}(\Theta,\Gamma)/\partial \ln \Theta$ increases with Θ and approaches $z \simeq 1$ for both island morphologies. This is consistent with a saturation (Θ-independence) of the island density for large Θ in the precoalescence regime, $\bar{s} \sim \Theta/N \sim \Theta$.

In the self-consistent theory,[14] the capture numbers are given by

$$\sigma_s^{\mathrm{sc}} = \frac{2\pi}{(1-\Theta)} \frac{R_s}{\xi} \frac{K_1(R_s/\xi)}{K_0(R_s/\xi)}, \tag{10a}$$

$$\xi^{-2} = 2\sigma_1^{\mathrm{sc}} n_1 + \sum_{s \geqslant 2} \sigma_s^{\mathrm{sc}} n_s\,, \tag{10b}$$

where R_s is the effective radius of an island of size s, K_0 and K_1 are the modified Bessel functions of order zero and one, respectively, and ξ is the adatom capture length (mean linear size of depletion zone around an island). The factor $(1-\Theta)$ in Eq. (10), which was not given in the original derivation in Ref. 14, arises from the fact that the adatom current to a (circular) island of size s is $2\pi R_s D\, \partial_r \tilde{n}_1(r)|_{r=R_s}$, where $\tilde{n}_1(r) = n_1(r)/(1-\Theta)$ is the adatom density with respect to the free (uncovered) surface area, and $n_1(r)$ is the local form corresponding to the global mean value n_1 appearing in the RE [see also Ref. 45 for the additional factor $(1-\Theta)$]. For $R_s \ll \xi$, $\sigma_s \sim 2\pi/[(1-\Theta)\ln(\xi/R_s)]$ and for $R_s \gg \xi$, $\sigma_s \sim 2\pi/(1-\Theta)(R_s/\xi)$.

To determine the σ_s^{sc}, the REs (1) and (2) are numerically solved with initial conditions $n_s = 0$ at time $t = 0$ and a cutoff value s_c so that n_s can be safely neglected for $s > s_c$. In each integration step the implicit Eq. (10) is solved for the σ_s^{sc}. The results become sensitive to the island morphology via the

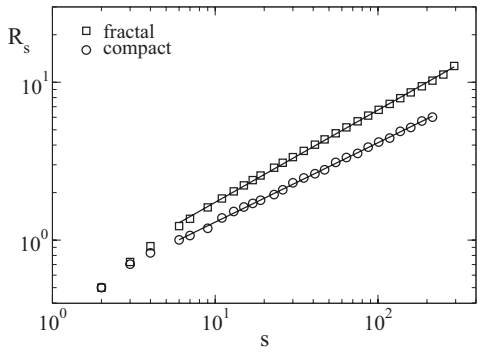

FIG. 3. Mean radii of gyration R_s of islands of size s for the models representing compact and fractal island morphologies. The straight lines in the double-logarithmic plot indicate the power-law behavior for large s.

dependence of R_s on s in this approach. For point islands we take $R_s = 1$ corresponding to one lattice constant. For the compact and fractal island morphologies, we determined the mean radius of gyration of islands of size s, as shown in Fig. 3. The straight lines in the double-logarithmic representation give $R_s \sim 0.42s^{1/2}$ (compact islands) and $R_s \sim 0.47s^{0.57}$ (fractal morphologies) for large s. To compare the $\sigma_s^{\rm sc}$ with the σ_s obtained from the KMC simulations, we used the full dependence of the R_s on s, i.e., including the small s behavior, in our integration of the RE. The results from the self-consistent theory are shown in Fig. 1 (open symbols). As can be seen from the figure, the $\sigma_s^{\rm sc}$ deviate strongly from the KMC results, both in their size and in their functional form. In particular, the self-consistent theory underestimates the capture numbers for large s, as known from earlier work in the literature.[3]

It is interesting to see, whether the scaling of $(1-\Theta)\sigma_s(\Theta,\Gamma)$ with R_s/ξ is valid, if the σ_s and n_s from the KMC simulations are used in the expression for ξ^{-2} in Eq. (10b). In this case, the linearization step used in this theory for deriving a linear diffusion equation for the local adatom density $n_1(r)$ could be reasoned, i.e., the step, where the term $2\sigma_1 n_1(r)^2 + \sum_{s>1}\sigma_s n_1(r) n_s(r)$ is replaced by $n_1(r)\xi^{-2}$ with $\xi^{-2} = 2\sigma_1 n_1 + \sum_{s>1}\sigma_s n_s$ given by the mean (r-independent) densities (see Ref. 14 for details). In Fig. 4, $(1-\Theta)\sigma_s(\Theta,\Gamma)$ is plotted as a function of R_s/ξ for the models representing compact and fractal island morphologies. Figure 4(a) shows that indeed a data collapse is obtained for different Γ values at fixed Θ. However, with respect to the Θ dependence, tested in Fig. 4(b), no scaling behavior is found. This indicates that the linearization step in the self-consistent theory leads to the unsatisfactory capture numbers. It has been shown that correlation effects between island sizes and capture areas need to be taken into account to improve theories for capture numbers and island size distributions. This can been achieved by considering the joint probability of island size and capture area.[42,45–48]

IV. ADATOM AND ISLAND DENSITIES

Numerical integration of the RE with the κ_s and σ_s from Sec. III gives an excellent description of the adatom density n_1 and of the island density N as a function of Θ and Γ for all island morphologies in the precoalescence regime. This is demonstrated in Fig. 5 where n_1 and N from the KMC simulation (open squares) and RE solution (solid lines) are plotted as a function of Θ for $\Gamma = 10^7$. For compact and fractal island morphologies, the KMC data for N steeply fall for coverages larger than 15% (compact islands) and 30% (fractal islands) because of island coalescences. Small deviations of the RE solution for n_1 can be seen close to its maximum, where it slightly underestimates the adatom density. The agreement for the other simulated Γ values is of the same quality. As known from previous studies,[1,11,14,45] the RE predict n_1 and N quite well also, when using the self-consistent capture numbers from Eq. (10). The corresponding solutions are drawn as dashed lines in Fig. 5. In view of the discrepancies discussed in Sec. III, this good predictive power of the RE under use of the self-consistent capture numbers $\sigma_s^{\rm sc}$ is surprising.

V. ISLAND SIZE DISTRIBUTIONS

Since the $\sigma_s^{\rm sc}(\Theta,\Gamma)$ deviate strongly from the $\sigma_s(\Theta,\Gamma)$, the RE with self-consistent capture numbers fail to predict the ISD. This failure was reported already when the self-consisting theory was developed.[14] In the following, we therefore do no longer consider the self-consistent theory, but concentrate

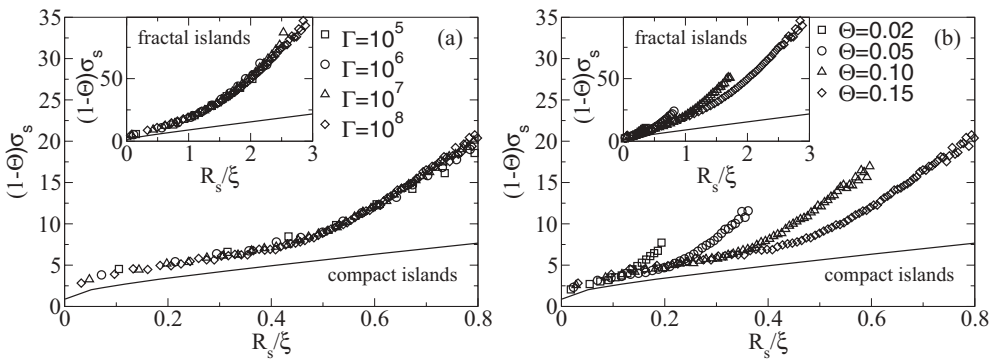

FIG. 4. Scaling plot of $(1-\Theta)\sigma_s$ as a function of R_s/ξ for the model representing compact island morphologies, with both R_s and $\xi^{-2} = 2\sigma_1 n_1 + \sum_{s\geqslant 2}\sigma_s n_s$ determined from the KMC simulations, (a) for various Γ and fixed $\Theta = 0.2$ and (b) for various Θ and fixed $\Gamma = 10^8$. The insets in (a) and (b) show the corresponding results for the model representing fractal island morphologies. The solid lines represent the specific functional form in Eq. (10) predicted by the self-consistent theory.

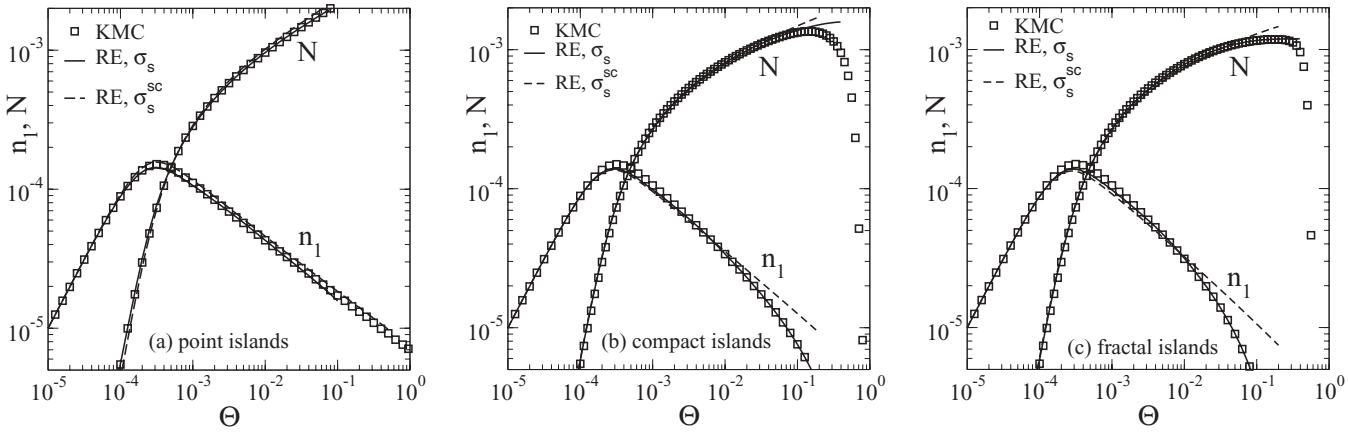

FIG. 5. KMC results (symbols) for the adatom density n_1 and island density N as function of Θ at $\Gamma = 10^7$ for (a) point, (b) compact, and (c) fractal island morphologies in comparison with the RE solutions, when using the direct capture areas κ_s and capture numbers σ_s from Sec. III (solid lines) and when using the capture numbers σ_s^{sc} from the self-consistent theory according to Eq. (10) (dashed lines).

on the principal questions whether the RE with the capture numbers $\sigma(\Theta,\Gamma)$ are successful in predicting the ISD, and if so, whether in the limit $\Gamma \to \infty$ the asymptotic form (7) for the scaling function becomes valid. In this section, we address the first of these two questions.

Representative results for the ISD (symbols) in comparison with the RE predictions are shown in Fig. 6 for $\Gamma = 10^7$ and three different coverages Θ, for point and fractal island morphologies. The excellent agreement between the RE predictions and the KMC data in that figure is also found for the other simulated Γ values. As was shown in Ref. 13 for the fractal island morphologies, a χ^2 test with a standard significance level of 5% is passed up to a coverage of $\Theta = 0.18$. For larger Θ, coalescence events, not included in the RE approach, become relevant.

For the compact island morphologies, a good agreement of the KMC data with the RE prediction is obtained up to coverages of about $\Theta = 0.05$ only, see Fig. 7(a). The reason for the discrepancies are coalescence events that become important already for small $\Theta \gtrsim 0.05$, in contrast to what one may conclude from the behavior of the mean island density shown in Fig. 5, where coalescences seem to be irrelevant up to coverages of about 15%. One can take out the coalescence effect in the calculation of the ISD by following the islands in the simulations and by counting coalesced islands as if they were separated. The islands identified in this way were referred to as subislands and the resulting ISD as sub-ISD in Refs. 3 and 40. In the same way as described in Sec. II, we determined the κ_s' and σ_s' for the subislands and integrated the REs (1) and (2) with these input quantities. As shown in Fig. 7(b), these RE results for the sub-ISD give again excellent agreement with the KMC data.

That coalescence events are much more frequent for compact than for fractal islands is shown in Fig. 8, where we plotted the fraction of the coalesced islands as a function of Θ both for the compact and fractal island morphologies. This fraction was determined by dividing the total number of coalescences up to the coverage Θ by the total number of islands at this Θ value, i.e., islands that have undergone more than one coalescence are counted with their corresponding multiplicities. As can be seen from Fig. 8, the fraction of coalesced islands for compact islands has already at $\Theta = 0.05$ reached a level comparable to that found for the fractal islands at $\Theta = 0.2$.

The reason for the less frequent coalescences of fractal islands is that two approaching fractal islands can avoid each other for some time, because fingers of one islands grow into breaches between fingers of the other island. When a finger enters a breach, its further growth slows down because of the shielding inside the breach. This screening effect and its consequence for coalescences has been discussed earlier in the literature.[1,37] A quantitative analysis of the coalescence

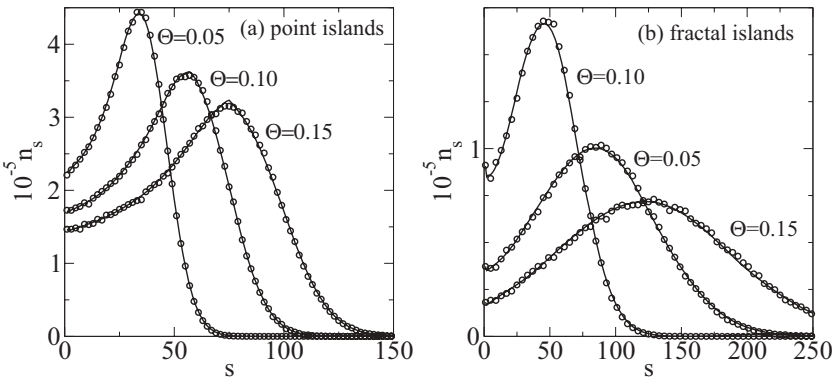

FIG. 6. Simulated island size distribution (circles) in comparison with the RE solution (lines) for three different Θ at $\Gamma = 10^7$ for the models representing (a) point and (b) fractal island morphologies.

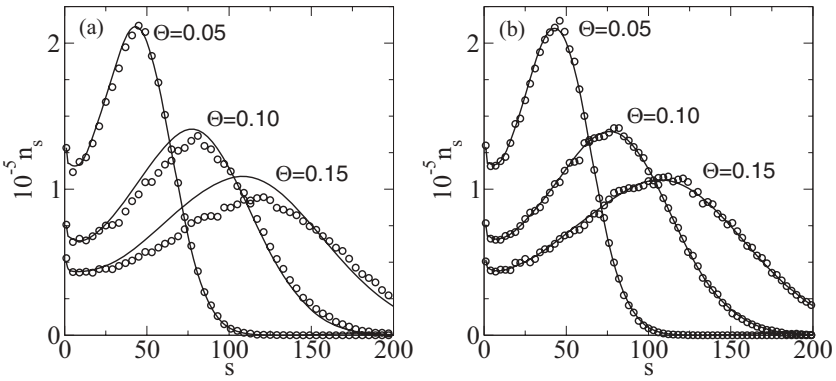

FIG. 7. (a) ISD and (b) sub-ISD for compact islands obtained from the KMC simulations (circles) in comparison with the RE solution (lines) for $\Gamma = 10^7$ and three different coverages Θ.

behavior of compact and fractal island morphologies is given in Appendix B.

VI. LIMITING BEHAVIOR FOR $\Gamma \to \infty$

Based on our first key finding that for all morphologies and for all coverages in the pre-coalescence regime, the ISDs from the KMC simulations are successfully predicted by the RE we now turn to the question, whether the scaled ISDs approach the asymptotic form (7) in the limit $\Gamma \to \infty$.

To answer this question is not easy because of various subtleties, which let us revisit the derivation of the scaling function by Bartelt and Evans[16,17] in Appendix A. As mentioned in Introduction, Eq. (4) for the limiting curve of the scaled ISD $f_\infty(x)$ should be valid if $f_\infty(x,\Theta)$ from Eq. (5) is independent of Θ. This is the case if $C_\infty(x,\Theta) = \lim_{\Gamma\to\infty} \sigma_{x\bar{s}}(\Theta,\Gamma)/\bar{\sigma}(\Theta,\Gamma)$ for the scaled capture numbers and $z_\infty(\Theta) = \lim_{\Gamma\to\infty} \partial \ln \bar{s}(\Theta,\Gamma)/\partial \ln \Theta$ also have Θ-independent limits. A further requirement for the validity of Eq. (7) is that $\lim_{\Gamma\to\infty} \bar{\kappa}(\Theta,\Gamma)/\bar{s}(\Theta,\Gamma) = 0$, where $\bar{\kappa} = N^{-1}\sum_{s>1} \kappa_s n_s$ is the mean direct capture area. This condition can be expected to be fulfilled for compact and point island morphologies and is in fact the reason, why the scaling function of the direct capture areas should not enter the RE prediction (7). If $\lim_{\Gamma\to\infty} \bar{\kappa}(\Theta,\Gamma)/\bar{s}(\Theta,\Gamma) > 0$, $f_\infty(x,\Theta)$ can be expected to depend on Θ and one would need to solve the semi-linear partial differential equation (A6) for $f_\infty(x,\Theta)$. Note that the κ_s cannot increase stronger than linearly with s, and accordingly $\bar{\kappa}$ should not increase more than linearly with $\bar{s}$.

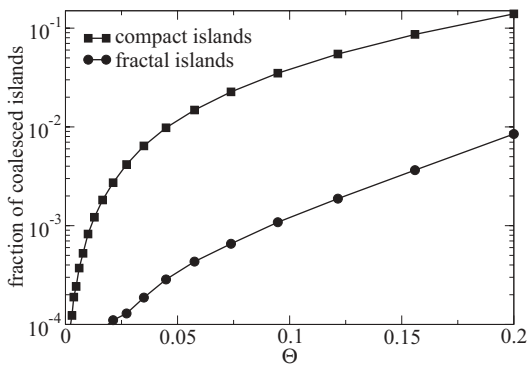

FIG. 8. Fraction of coalesced islands as a function of the coverage Θ for $\Gamma = 10^7$.

In interpreting numerical results for finite Γ, we have to pay attention to the fact that for smaller Θ larger Γ values are needed to approach the limiting curves. This is because $\bar{s}(\Theta,\Gamma)$ must become large enough to reach the "continuum limit" (and larger Γ are needed to obtain the same $\bar{s}$ at smaller Θ), and because the relation $n_1 \sim (1-\Theta)/\Gamma\bar{\sigma}N$, used in the derivation of Eq. (7), should be obeyed. This relation is usually referred to as the quasistationary condition, since it follows from balancing the adatom attachment rate $D\bar{\sigma}nN$ to islands with the deposition rate $F(1-\Theta)$. However, as was shown earlier,[44] the relation is also valid for small Θ values in the regimes, where relative changes of N are still large and have not leveled off. A refined scaling analysis yields that, for $i = 1$ as relevant here, the relation holds for $(\Theta^2\Gamma)^{1/3} \gg 1$, implying again that for smaller Θ larger Γ are needed to identify the limiting behavior.

Figure 9 shows $n_s\bar{s}^2/\Theta$ as a function of $s/\bar{s}$ for $\Gamma = 10^8$ at four different coverages for the (a) point and (b) fractal island morphologies. In the insets, the scaled ISDs are shown for a fixed coverage $\Theta = 0.2$ and different Γ. In the case of the point island morphologies, the data suggest the existence of a Θ-independent limiting curve, in agreement with previous findings.[3] For the fractal island morphologies, the scaled ISD for different Θ show no clear signature of a Θ-independent limiting curve. Based on the tendency of the simulated data for different Θ and Γ to become slightly closer to each other for larger Θ and Γ, one may conjecture that also in this case a limiting curve would be reached at larger Γ values. However, the fact that for each fixed Θ, the curves at large Γ are almost overlapping suggests that these are good estimates of $f_\infty(x,\Theta)$. Our conclusion is therefore that it is not likely that a Θ-independent limiting curve exists for the hit-and-stick model used here for the fractal island morphologies.

This conclusion is further corroborated by the fact that the scaled direct capture areas exhibit a nearly linear dependence on x for the fractal islands (not shown). Thus we encounter the case here, where the scaled direct capture areas $\bar{\kappa}(\Theta,\Gamma)/\bar{s}(\Theta,\Gamma)$ appear to approach a non-vanishing limit for $\Gamma \to \infty$, which would mean that in a strict treatment, Eq. (7) can no longer be applied. If one considers $f_\infty(x,\Theta)$ to depend only very weakly on Θ, $\partial f_\infty(x,\Theta)/\partial\Theta \simeq 0$, we could replace $C_\infty(x)$ by $C_{\rm tot}(x) = C_\infty(x) + \rho_\infty\Theta K_\infty(x,\Theta)/(1-\Theta)$, where $K_\infty(x,\Theta) = \lim_{\Gamma\to\infty} \kappa_{x\bar{s}}(\Theta,\Gamma)/\bar{\kappa}(\Theta,\Gamma)$ is the limiting curve for the scaled direct capture areas and $\rho_\infty = \lim_{\Gamma\to\infty} \bar{\kappa}(\Theta,\Gamma)/\bar{s}(\Theta,\Gamma) > 0$.

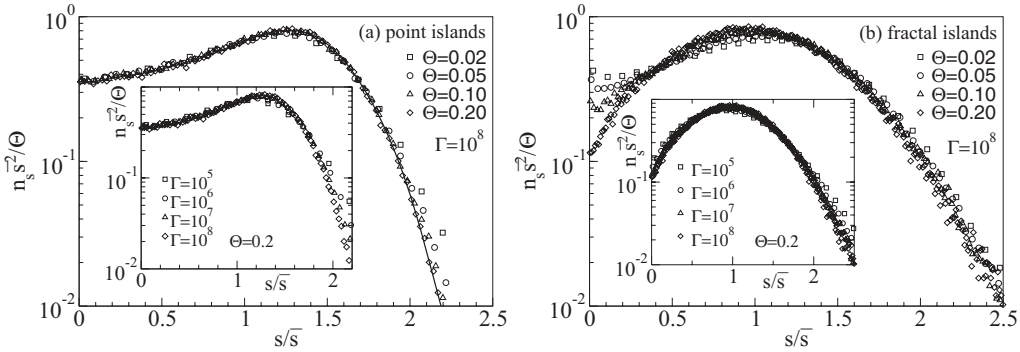

FIG. 9. Scaled island size distributions $n_s\bar{s}^2/\Theta$ as function of the scaled island size $x = s/\bar{s}$ for fixed $\Gamma = 10^8$ and four coverages Θ, for (a) point and (b) fractal island morphologies. The insets show the scaled ISDs at fixed $\Theta = 0.2$ and the four simulated Γ values. The line in (a) is a fit to the data for $\Theta = 0.2$ and $\Gamma = 10^8$ and agrees with the analytical result Eq. (7), when using the line in Fig. 10(a) as the estimate for $C_\infty(x)$.

Our conclusions drawn with respect to the scaled ISDs of the point islands are consistent with the behavior of the scaled capture numbers, which are shown in Fig. 10(a) for the same Θ and Γ values as in Fig. 9(a). In this Fig. 10(a), an approach to a Θ-independent limiting curve $C_\infty(x)$ can be seen. In the case of the fractal island morphologies by contrast, an approach to a Θ-independent limiting curve cannot be clearly identified, which gives further evidence that the $f_\infty(x,\Theta)$ are dependent on Θ.

In order to test the validity of Eq. (7) for the point islands, we set $z_\infty = 2/3$ (see Sec. III) and used a fit to the scaled ISD for $\Gamma = 10^8$ and $\Theta = 0.2$ in Fig. 9(a) as an estimate for $f_\infty(x)$. The fit, which fulfills the constraints of normalization and normalized first moment, is shown as line in this figure. We then estimated $C_\infty(x)$ based on this fit by rewriting Eq. (A6) from Appendix A [for Θ-independent $f_\infty(x)$] in the form

$$\frac{dC_\infty(x)}{dx} = (2z_\infty - 1) - [C_\infty(x) - z_\infty x]\frac{d\ln[f_\infty(x)]}{dx}. \quad (11)$$

Since the solution of this differential equation is proportional to $1/f_\infty(x)$, we preferred to integrate Eq. (11) with the initial condition $C_\infty(0) = f_\infty(0)/(1 - z_\infty)$ to achieve a stable numerical results for large x also. The resulting estimate for $C_\infty(x)$ is shown as line in Fig. 10(a). The line lies slightly above the data for the scaled capture numbers for $\Gamma = 10^8$ and $\Theta = 0.2$, indicating that indeed an estimate of a limiting curve for the scaled capture numbers is obtained. In a cross check, we performed the integral in Eq. (7) with the estimated $C_\infty(x)$ and recovered the line in Fig. 9(a).

For the compact island morphologies, Eq. (7) would be of limited practical use, because, as discussed in Sec. V, the REs (1) and (2) fail to predict the ISD correctly already at small Θ due to coalescences. Nevertheless, from a conceptual viewpoint, it is interesting to study the scaled ISD and their relation to the scaled capture numbers for the subislands. The corresponding data shown in Fig. 11 indicate a behavior similar as for the fractal island morphologies, where the limiting curves are dependent on Θ.

VII. SUMMARY

The capture numbers entering the RE for the growth kinetics of thin films have been determined by KMC simulations in their dependence on both the coverage Θ and the $\Gamma = D/F$ ratio for the point island model and for two simple growth models representative for islands with compact and fractal shapes. It was shown that the Θ dependence of the capture numbers could not be accounted for by the ratio R_s/ξ of the mean island radius R_s and the effective adatom capture length ξ of the RE. This suggests that the strong deviations

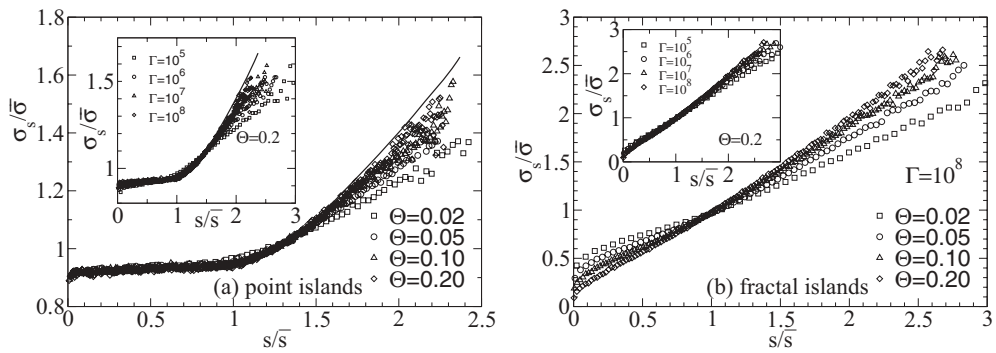

FIG. 10. Scaled capture numbers $\sigma_s/\bar{\sigma}$ as function of the scaled island size $s/\bar{s}$ for fixed $\Gamma = 10^8$ and four coverages Θ, for (a) point and (b) fractal island morphologies. The insets show the scaled capture numbers at fixed $\Theta = 0.2$ and the four simulated Γ values. The line in (a) marks the solution obtained from a numerical integration of Eq. (11) when using the fit (line) to the scaled ISDs curve for $\Gamma = 10^8$ and $\Theta = 0.2$ in Fig. 9(a).

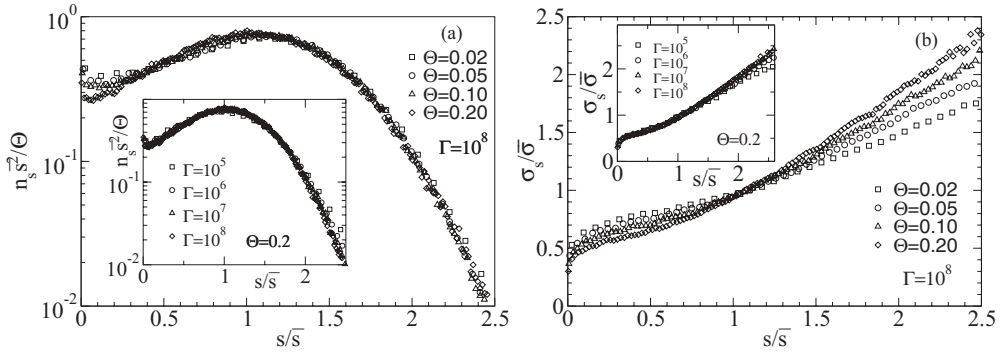

FIG. 11. (a) Scaled island size distributions and (b) scaled capture numbers of subislands as function of the scaled island size in the case of compact island morphologies for fixed $\Gamma = 10^8$ and four coverages Θ. The inset shows the corresponding data at fixed $\Theta = 0.2$ and the four simulated Γ values.

between the capture numbers determined from the simulations and the ones predicted by the self-consistent theory have their origin in the linearization step used in this theory. The RE with self-consistent capture numbers nevertheless provide a good quantitative account of the adatom and island density. The deviations to the correct capture numbers lead, however, to a failure for a description of the ISD.

Integration of the RE with the simulated capture numbers determined from the KMC simulations gives an excellent quantitative prediction of the ISDs. For the compact islands morphologies, it was found that coalescence events, not considered in the RE, become relevant already at small coverages well below $\Theta \simeq 0.15$, where coalescence events do not significantly affect the island density. Compared to the fractal island morphologies, the coalescence rate for the compact morphologies is much higher. The ISD is affected already by a rather small number of coalescences, because these lead to a reshuffling of weights for different island sizes. The lower coalescence rate for fractal morphologies is caused by the fact that fingers of two approaching fractal islands typically first avoid each other, which subsequently leads to a screening effect and a slowing down of further growth of these fingers.

Finally, we discussed the limiting curves for the scaled ISDs when $\Gamma \to \infty$. For the point islands the KMC data provide evidence that these limiting curves are independent of the coverage, which is given by the RE prediction (7). This means that there exists a true scaling behavior in the $\Gamma \to \infty$ limit, where the dependence on Θ is fully accounted for by the mean island size $\bar{s}$. For the growth models representing compact and fractal island morphologies, the results indicate that the limiting curves are dependent on Θ. This implies that one needs to solve the partial differential equation (A6) [or Eq. (A10)] to calculate $f_\infty(x,\Theta)$ from $C_\infty(x,\Theta)$. Unfortunately, no successful theory exists so far to predict the limiting curve $C_\infty(x,\Theta)$ for the scaled capture numbers.

The limiting curves are also different for different morphologies. Considering how sensitive the shape of the limiting curves depends on the nonlinear behavior of the scaled capture numbers as a function of the scaled island size, it is well possible that the shape will also vary with details of the growth mechanisms, even if the type of island morphology remains essentially the same.

APPENDIX A: RATE EQUATION PREDICTION OF THE LIMITING CURVES FOR THE SCALED ISLAND SIZE DISTRIBUTION

For large Γ, $\bar{s} \sim N^{-1} \sim \Gamma^{1/3}$ and $x = s/\bar{s}$ becomes a continuous variable, which allows one to derive a determining equation for the scaled ISD in dependence of the scaled capture numbers. The derivation was first presented by Bartelt and Evans.[16,17] Replacing the variable s by x and using $\partial/\partial(Ft) = (1-\Theta)\partial/\partial\Theta$, Eq. (2) can be written in the continuum limit as

$$\frac{\partial n_{x\bar{s}}}{\partial\Theta} = -\frac{1}{(1-\Theta)\bar{s}}\left[\Gamma n_1 \frac{\partial}{\partial x}(\sigma_{x\bar{s}} n_{x\bar{s}}) + \frac{\partial}{\partial x}(\kappa_{x\bar{s}} n_{x\bar{s}})\right]. \quad \text{(A1)}$$

Defining $f(x,\Theta,\Gamma) = \bar{s}^2 n_{x\bar{s}}/\Theta$, $C(x,\Theta,\Gamma) = \sigma_{x\bar{s}}/\bar{\sigma}$, and $K(x,\Theta,\Gamma) = \kappa_{x\bar{s}}/\bar{\kappa}$, one has

$$\frac{\partial}{\partial x}(\sigma_{x\bar{s}} n_{x\bar{s}}) = \frac{\Theta\bar{\sigma}}{\bar{s}^2}\frac{\partial(Cf)}{\partial x}, \quad \text{(A2)}$$

$$\frac{\partial}{\partial x}(\kappa_{x\bar{s}} n_{x\bar{s}}) = \frac{\Theta\bar{\kappa}}{\bar{s}^2}\frac{\partial(Kf)}{\partial x} \quad \text{(A3)}$$

$$\frac{\partial n_{x\bar{s}}}{\partial\Theta} = -(2z-1)f - zx\frac{\partial f}{\partial x} + \Theta\frac{\partial f}{\partial\Theta}, \quad \text{(A4)}$$

where $z(\Theta,\Gamma) = \partial \ln\bar{s}/\partial\ln\Theta$. The reduced RE moreover predict $n_1 \sim (1-\Theta)/(\Gamma\bar{\sigma}N) \sim (1-\Theta)\bar{s}/(\Theta\Gamma\bar{\sigma})$ for large Γ and fixed $\Theta > \Theta_x \sim \Gamma^{-1/2}$. Inserting this relation and Eqs. (A2)–(A4) into Eq. (A1) gives

$$(2z-1)f + zx\frac{\partial f}{\partial x} - \Theta\frac{\partial f}{\partial\Theta} = \frac{\partial(Cf)}{\partial x} + \frac{\Theta\bar{\kappa}}{(1-\Theta)\bar{s}}\frac{\partial(Kf)}{\partial x}. \quad \text{(A5)}$$

Introducing the limits $C_\infty(x,\Theta) = \lim_{\Gamma\to\infty} C(x,\Theta,\Gamma)$, $K_\infty(x,\Theta) = \lim_{\Gamma\to\infty} K(x,\Theta,\Gamma)$ and $z_\infty(\Theta) = \lim_{\Gamma\to\infty} z(\Theta,\Gamma)$, Eq. (A5) yields a determining equation for $f_\infty(x,\Theta) = \lim_{\Gamma\to\infty} f(x,\Theta,\Gamma)$.

For $\lim_{\Gamma\to\infty}\bar{\kappa}/\bar{s} = 0$, one obtains

$$(2z_\infty - 1)f_\infty + z_\infty x\frac{\partial f_\infty}{\partial x} - \Theta\frac{\partial f_\infty}{\partial\Theta} = \frac{\partial(C_\infty f_\infty)}{\partial x}. \quad \text{(A6)}$$

The condition $\lim_{\Gamma\to\infty}\bar{\kappa}/\bar{s} = 0$ is valid for point islands, and it can be expected to hold also for compact island morphologies unless atoms deposited on top of islands are essentially all attaching to the island edge in the first layer (a situation unlikely due to second layer nucleation on larger islands).

When integrating Eq. (A6) over x from zero to infinity, the first, second, and third terms on the left-hand side yield $(2z_\infty - 1)$, z_∞ (after a partial integration) and zero, respectively, because of the normalization of f_∞. The right-hand side becomes $[-C_\infty(0,\Theta) f_\infty(0,\Theta)]$ (note that for large x, $C_\infty \sim x$, and f_∞ must decrease faster than x to be normalizable—simulation results show that f_∞ should in fact decay much faster). Accordingly, the relation

$$f_\infty(0,\Theta) = \frac{1 - z_\infty(\Theta)}{C_\infty(0,\Theta)} \tag{A7}$$

must be fulfilled. A corresponding relation can be derived in the same way already from Eq. (A5). Analogously, when first multiplying Eq. (A6) with x and then integrating, one obtains

$$\int_0^\infty C_\infty(x,\Theta) f_\infty(x,\Theta) = 1\,. \tag{A8}$$

Integrating Eq. (A6) to a finite value x then yields

$$C_\infty(x,\Theta) = z_\infty(\Theta)x + \frac{1 - z_\infty(\Theta)}{f_\infty(x,\Theta)} \int_x^\infty dx'\, f_\infty(x',\Theta) - \frac{\Theta}{f_\infty(x,\Theta)} \frac{\partial}{\partial\Theta} \int_0^x dx'\, f_\infty(x',\Theta)\,, \tag{A9}$$

which expresses $C_\infty(x,\Theta)$ as a functional of $f_\infty(x,\Theta)$.

When one further assumes that the limiting curve f_∞ is independent of Θ, one has $\partial f_\infty/\partial\Theta = 0$ and can neglect the corresponding term in Eq. (A5). For self-consistency, this requires also C_∞ and z_∞ to become independent of Θ. In fact, one can conversely show that if C_∞ and z_∞ are independent of Θ, f_∞ must by independent of Θ also. Under this assumption Eq. (A6) then reduces to a separable ordinary differential equation, whose solution is given by Eq. (7), with $C_{\rm tot}(x)$ equal to $C_\infty(x)$ and z equal to z_∞.

If there exists a finite limit $\rho_\infty(\Theta) = \lim_{\Gamma\to\infty} \bar\kappa/\bar s > 0$, as it may be the case for fractal island morphologies (see the discussion in Sec. VI), Eq. (A5) yields

$$(2z_\infty - 1) f_\infty + z_\infty x \frac{\partial f_\infty}{\partial x} - \Theta \frac{\partial f_\infty}{\partial\Theta} = \frac{\partial(C_\infty f_\infty)}{\partial x} + \rho_\infty \frac{\Theta}{(1-\Theta)} \frac{\partial(K_\infty f_\infty)}{\partial x} \tag{A10}$$

as determining equation for $f_\infty(x,\Theta)$. Strictly speaking, a Θ-independent $f_\infty(x)$ should not exist then, and one needs to solve the semilinear partial differential equation (A10). If one nevertheless makes the approximation $\partial f_\infty/\partial\Theta \simeq 0$ in Eq. (A10) and considers C_∞ and z_∞ to be independent of (or only weakly dependent on) Θ, one would obtain the weakly Θ-dependent solution Eq. (7) with $C_{\rm tot} = C_\infty + \rho_\infty \Theta K_\infty/(1-\Theta)$.

APPENDIX B: QUANTITATIVE ANALYSIS OF COALESCENCE EVENTS

For a quantitative analysis of the coalescence behavior, we determined the fraction of pair distance vectors of coalescing islands that before coalescence exhibit an antiparallel orientation to the vector connecting the center of masses of the islands. Let us denote by $\mathbf{R}_{i,j}$ the vector pointing from the center of mass of island i to the center of mass of island j, and by $\mathbf{r}_{i\alpha,j\beta}$ the vector pointing from atom α of island i to atom β of island j. The fraction of distance vectors with antiparallel orientation then is

$$\Phi_{ij} = \frac{1}{s_i s_j} \sum_{\alpha,\beta} H(-\mathbf{r}_{i\alpha,j\beta} \cdot \mathbf{R}_{i,j})\,, \tag{B1}$$

where $H(.)$ is the Heaviside jump function with $H(x) = 1$ for $x > 0$ and zero else. For a given time lag Δt before coalescence, the Φ_{ij} were averaged over all coalescence events, yielding the mean fraction $\Phi(\Delta t)$ of distance vectors with anti-parallel orientation. To obtain the corresponding data, configurations generated by the KMC simulations were analyzed afterwards back in time, starting from the instant where islands first touched each other.

The mean fraction Φ obtained from this analysis is shown in Fig. 12(a) as a function of Δt for $\Gamma = 10^7$. We assigned negative values to Δt to emphasize that $\Phi(\Delta t)$ was determined for lags before a coalescence event. That $\Phi(\Delta t)$ for fractal islands is by many orders of magnitude larger than for compact islands demonstrates the partial inter-penetration of the fractal islands before coalescence. The value $\Phi(\Delta t) \simeq 0.01$ reached for the fractal island morphologies in the limit $\Delta t \to 0$ means that on average about 10% of the atoms of each island in a coalescence event pass each other. That the partial inter-penetration is accompanied by a slowing down of the approach of two islands before coalescence can be seen in Fig. 12(b), where the averaged minimal distance $d(\Delta t)$ between coalescing islands is shown, that means $d_{ij} = \min_{\alpha,\beta}(|\mathbf{r}_{i\alpha,j\beta}|)$ averaged over all coalescences of islands i and j for time lag Δt. The (negative) slope of $d(\Delta t)$ is significantly smaller for the fractal island morphologies, giving evidence for the screening effect.[1,37]

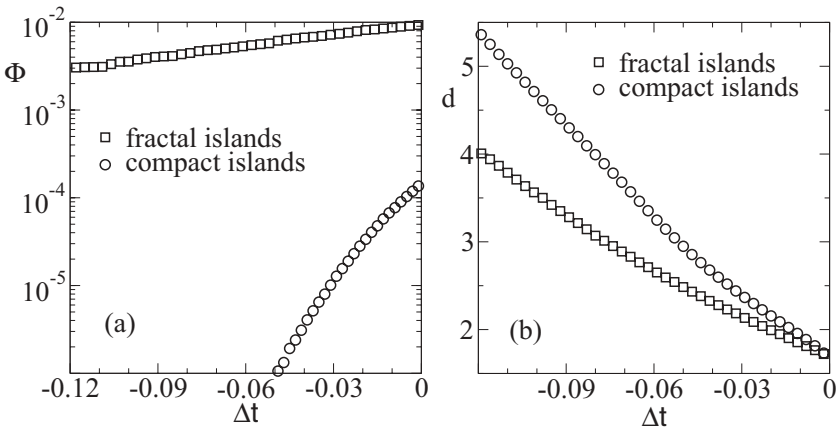

FIG. 12. (a) Mean fraction Φ of distance vectors with antiparallel orientation (with respect to the center of mass distance vector) and (b) mean minimal distance d between islands as a function of the time lag $\Delta t < 0$ before a coalescence event at zero time. The times are given in units of F^{-1} and the data were determined from the KMC simulations for $\Gamma = 10^7$.

*mario.einax@uni-osnabrueck.de
†philipp.maass@uni-osnabrueck.de;
http://www.statphys.uni-osnabrueck.de

[1] H. Brune, Surf. Sci. Rep. **31**, 125 (1998).
[2] T. Michely and J. Krug, *Islands, Mounds and Atoms: Patterns and Processes in Crystal Growth far from equilibrium* (Springer, Berlin, 2004).
[3] J. W. Evans, P. A. Thiel, and M. C. Bartelt, Surf. Sci. Rep. **61**, 1 (2006).
[4] W. Dieterich, M. Einax, and P. Maass, Eur. Phys. J. Special Topics **161**, 151 (2008).
[5] J. A. Venables, Phil. Mag. **27**, 697 (1973).
[6] G. Hlawacek, P. Puschnig, P. Frank, A. Winkler, C. Ambrosch-Draxl, and C. Teichert, Science **321**, 108 (2008).
[7] F. Loske, J. Lübbe, J. Schütte, M. Reichling, and A. Kühnle, Phys. Rev. B **82**, 155428 (2010).
[8] A. Zangwill and D. D. Vvedensky, Nano Lett. **11**, 2092 (2011).
[9] T. Potocar, S. Lorbek, D. Nabok, Q. Shen, L. Tumbek, G. Hlawacek, P. Puschnig, C. Ambrosch-Draxl, C. Teichert, and A. Winkler, Phys. Rev. B **83**, 075423 (2011).
[10] M. Körner, F. Loske, M. Einax, A. Kühnle, M. Reichling, and P. Maass, Phys. Rev. Lett. **107**, 016101 (2011).
[11] C. Ratsch and J. A. Venables, J. Vac. Sci. Technol. A **21**, S96 (2003).
[12] When starting from a many-particle master equation for the growth kinetics of interacting adsorbate particles, the nonlinear terms in the rate equations would arise from some mean-field treatment of higher order correlation functions of occupations numbers, see, for example, J.-F. Gouyet *et al*., Adv. Phys. **52**, 523 (2003).
[13] M. Körner, M. Einax, and P. Maass, Phys. Rev. B **82**, 201401 (2010).
[14] G. S. Bales and D. C. Chrzan, Phys. Rev. B **50**, 6057 (1994).
[15] G. S. Bales and A. Zangwill, Phys. Rev. B **55**, R1973 (1997).
[16] M. C. Bartelt and J. W. Evans, Phys. Rev. B **54**, R17359 (1996).
[17] J. W. Evans and M. C. Bartelt, Phys. Rev. B **63**, 235408 (2001).
[18] J. A. Venables, G. D. T. Spiller, and M. Hanbucken, Rep. Prog. Phys. **47**, 399 (1984).
[19] J. A. Venables, Surf. Sci. **299–300**, 798 (1994).
[20] M. Einax, S. Ziehm, W. Dieterich, and P. Maass, Phys. Rev. Lett. **99**, 016106 (2007).
[21] M. Einax, W. Dieterich, and P. Maass, J. Appl. Phys. **105**, 054312 (2009).
[22] T. Vicsek and F. Family, Phys. Rev. Lett. **52**, 1669 (1984).
[23] D. D. Vvedensky, Phys. Rev. B **62**, 15435 (2000).
[24] J. G. Amar and F. Family, Phys. Rev. Lett. **74**, 2066 (1995).
[25] R. Ruiz, B. Nickel, N. Koch, L. C. Feldman, R. F. Haglund, A. Kahn, F. Family, and G. Scoles, Phys. Rev. Lett. **91**, 136102 (2003).
[26] J. M. Pomeroy and J. D. Brock, Phys. Rev. B **73**, 245405 (2006).
[27] A. Pimpinelli and T. L. Einstein, Phys. Rev. Lett. **99**, 226102 (2007).
[28] T. J. Oliveira and F. D. A. Aarão, Reis, Phys. Rev. B **83**, 201405 (2011).
[29] M. Li, Y. Han, and J. W. Evans, Phys. Rev. Lett. **104**, 149601 (2010).
[30] A. Pimpinelli and T. L. Einstein, Phys. Rev. Lett. **104**, 149602 (2010).
[31] F. G. Gibou, C. Ratsch, M. F. Gyure, S. Chen, and R. E. Caflisch, Phys. Rev. B **63**, 115401 (2001).
[32] F. Gibou, C. Ratsch, and R. Caflisch, Phys. Rev. B **67**, 155403 (2003).
[33] M. F. Gyure, C. Ratsch, B. Merriman, R. E. Caflisch, S. Osher, J. J. Zinck, and D. D. Vvedensky, Phys. Rev. E **58**, R6927 (1998).
[34] M. C. Bartelt, C. R. Stoldt, C. J. Jenks, P. A. Thiel, and J. W. Evans, Phys. Rev. B **59**, 3125 (1999).
[35] M. C. Bartelt, A. K. Schmid, J. W. Evans, and R. Q. Hwang, Phys. Rev. Lett. **81**, 1901 (1998).
[36] J. B. Hannon, M. C. Bartelt, N. C. Bartelt, and G. L. Kellogg, Phys. Rev. Lett. **81**, 4676 (1998).
[37] H. Brune, G. S. Bales, J. Jacobsen, C. Boragno, and K. Kern, Phys. Rev. B **60**, 5991 (1999).
[38] V. Holubec, P. Chvosta, M. Einax, and P. Maass, Europhys. Lett. **93**, 40003 (2011).
[39] D. T. Gillespie, J. Phys. Chem. **81**, 2340 (1977).
[40] M. C. Bartelt and J. W. Evans, Surf. Sci. **298**, 421 (1993).
[41] M. C. Bartelt, C. R. Stoldt, C. J. Jenks, P. A. Thiel, and J. W. Evans, Phys. Rev. B **59**, 3125 (1999).
[42] J. G. Amar, M. N. Popescu, and F. Family, Phys. Rev. Lett. **86**, 3092 (2001).
[43] M. C. Bartelt and J. W. Evans, Phys. Rev. B **46**, 12675 (1992).
[44] W. Dieterich, M. Einax, S. Heinrichs, and P. Maass, Fluctuation effects in kinetic thin film growth, in *Anomalous Fluctuation Phenomena in Complex Systems: Plasmas, Fluids, and Financial Markets*, edited by C. Riccardi and H. E. Roman (Transworld Research Network, Kerala, India, 2008), Chap. 8, pp. 211–244.
[45] M. N. Popescu, J. G. Amar, and F. Family, Phys. Rev. B **64**, 205404 (2001).
[46] P. A. Mulheran and D. A. Robbie, Europhys. Lett. **49**, 617 (2000).
[47] J. W. Evans and M. C. Bartelt, Phys. Rev. B **66**, 235410 (2002).
[48] P. A. Mulheran, Europhys. Lett. **65**, 379 (2004).